Chapter 2

Nonlinear flux loss from solar interior and its role in explaining the observed properties of solar cycle evolution

2.1 Introduction

In Chapter 1 we have discussed that the solar activity, as measured for example by the number of sunspots on the solar surface, varies in cyclic fashion with a period of around 11 years. The strength of each cycle (e.g., the maximum number of sunspots) also varies in a wide range from cycle to cycle. In this chapter, I would like to elaborate on one of the nonlinear mechanisms in the process of the build-up of the poloidal field from the toroidal component which plays a crucial role in saturating the cycle strengths and in regulating the statistical properties of the solar cycles (Biswas et al., 2022).

An interesting observation about the evolution of the solar cycles is that the strong and weak cycles have systematic differences: compared to weak cycles, strong cycles begin at higher latitudes, rise more rapidly, reach their maxima earlier and consequently have a longer decline phase (Waldmeier, 1935). This is known as the Waldmeier effect which has

also been confirmed in the reconstructed solar activity data over the millennial time scale (Usoskin et al., 2021) and even in other solar-type stars (Garg et al., 2019).

A stronger constraint is that all cycles behave in the same way towards the end of the cycle (Cameron and Schüssler, 2016, hereafter CS16). This phenomenon was first mentioned by Waldmeier (1955). This is illustrated in Figure 2.1, and we refer the reader to the work by Hathaway (2011) and CS16 for the observational analysis. In the upper panel of Figure 2.1, the three colored curves show the sunspot number for cycles of weak (blue), moderate (green) and high (red) levels of activity. The curves are based on the empirical curve-fitting of Hathaway et al. (1994b). The sunspots appear in butterfly wings, and the central latitude of the butterfly wings drift towards the equator in a way which is independent of cycle strength (black curve) Hathaway (2011). Finally, the width of the butterfly wings (light vertical lines) depends on the cycle strength early in the cycle but is independent of the cycle strength late in the cycle (Cameron and Schüssler, 2016). The properties of the butterfly diagram in the late phase of all the cycles are the same, i.e., all cycles die in the same way although they have different properties during the rise phase of the cycle (Cameron and Schüssler, 2016). Because all cycles drift towards the equator in the same way, the central latitude of the butterfly wings can be used as the independent variable rather than time from the start of the cycle as shown in the lower panel of Figure 2.1. The solid light lines indicate the width of the butterfly wings as a function of latitude. The dashed light lines are the upper limit for the width during the early phases of the cycle: the width increases as the cycle progresses until it reaches this level. Thereafter the cycle begins to decline.

The fact that the cycles all have the same statistical properties (in the amplitude vs spatial distribution plane) in the late phases of the cycle despite having different properties in the early phase of the cycle indicates a strong nonlinearity acting as the cycle progresses. The nonlinearity is particularly important because during the late phase of the cycle

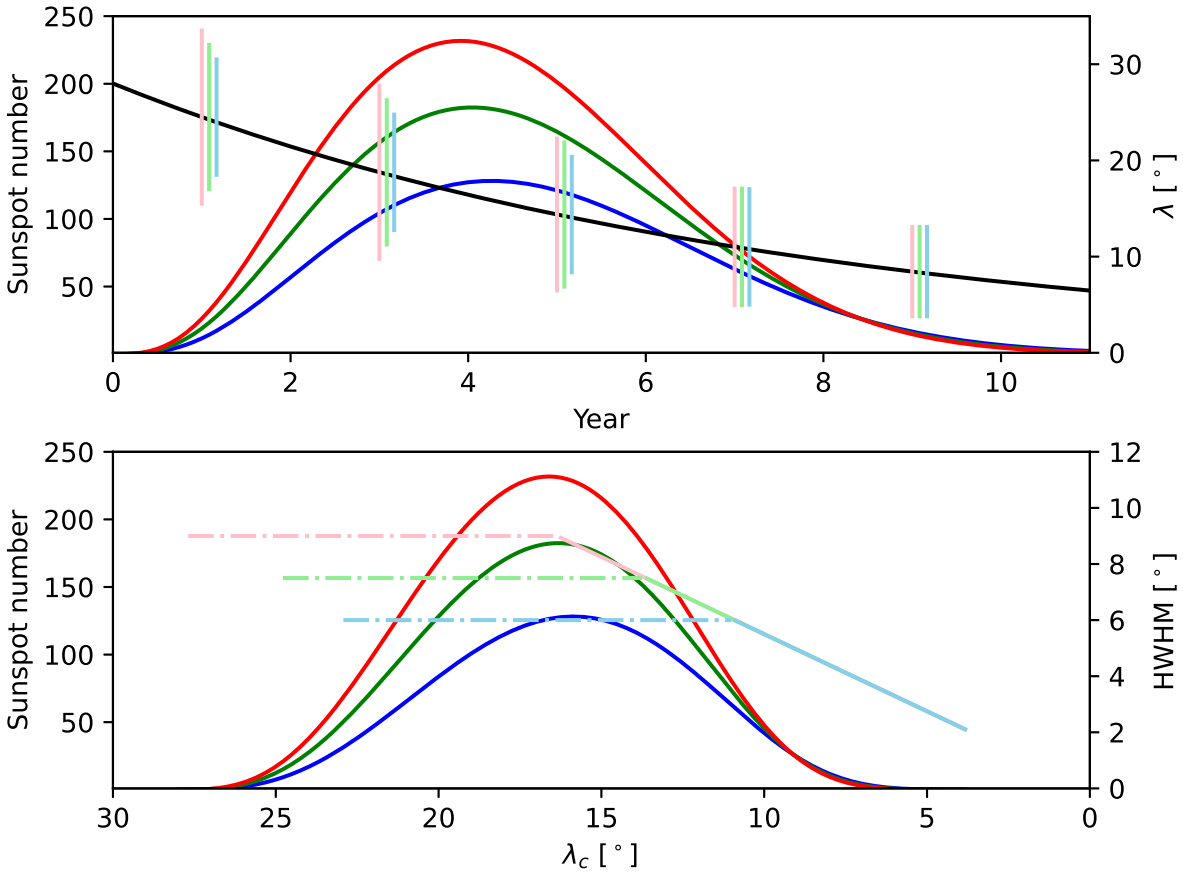

Fig. 2.1 Illustration of the behavior of cycles of different strengths based on the empirical solar cycle curve fitting of Hathaway et al. (1994b). Please refer to the text for the discussion regarding the properties of cycle evolution shown in the figure (Biswas et al., 2022). Image Credit: Biswas et al. (2022).

sunspots emerge closer to the equator and hence contribute more to the build-up of Sun's polar fields (Jiang, 2020; Karak, 2020; Petrovay et al., 2020). (The magnetic flux of the leading polarity of the bipolar magnetic regions (BMRs) that emerge closer to the equator gets easily carried across the equator by small-scale convective motions. It is the cross-equatorial cancellation of this flux that changes the net flux in each hemisphere and the polar fields at the end of each cycle (Durrant et al., 2004)). The nonlinearity hence leads to the change in polar field from one cycle to the next being only weakly dependent of the cycle strength Jiang (2020).

2.2 Model Description

In recent years, Babcock–Leighton type flux transport dynamo models have explained many features of the irregular solar cycle (Charbonneau, 2020; Karak, 2023). For example, Karak and Choudhuri (2011) explained the Waldmeier effect using a Babcock–Leighton type flux transport dynamo model. More recetly, Mandal et al. (2017) reproduced the basic correlations described above using a Babcock–Leighton dynamo model. However, why they were successful in this regard was not discussed. Here, we shall employ a Babcock–Leighton type dynamo model to explain the features reported by Waldmeier (1955) and CS16. We shall further show that in order to reproduce these features, some constraints on the nonlinearity in terms of the equipartition field strength, and the variation of meridional flow can be inferred.

For our study, we use an updated version of the code SURYA (Chatterjee et al., 2004; Nandy and Choudhuri, 2002), which solves the axisymmetric version of the mean-field dynamo equations as already mentioned in Chapter 1. However, for completeness, we reiterate the equations here again with the following discussion regarding the description of various parameters used in the model:

$$\frac{\partial A}{\partial t} + \frac{1}{s}(\vec{v}_p \cdot \vec{\nabla})(sA) = \eta_p \left(\nabla^2 - \frac{1}{s^2}\right) A + \alpha B, \tag{2.1}$$

$$\frac{\partial B}{\partial t} + \frac{1}{r}\left[\frac{\partial (r v_r B)}{\partial r} + \frac{\partial (v_\theta B)}{\partial \theta}\right] = \eta_t \left(\nabla^2 - \frac{1}{s^2}\right) B + s(\vec{B}_p.\vec{\nabla})\Omega + \frac{1}{r}\frac{d\eta_t}{dr}\frac{\partial (rB)}{\partial r} \tag{2.2}$$

where r is radial distance from the center of the Sun, θ is the co-latitude, $B(r,\theta)$ is the toroidal field and $A(r,\theta)$ is the ϕ component of the magnetic vector potential of the poloidal magnetic field $\vec{B}_p$, $s = r\sin\theta$, $\vec{v}_p = v_r\hat{r} + v_\theta\hat{\theta}$ is the meridional circulation, $\Omega(r,\theta)$ is the local rotation rate, $\eta_p(r)$ and $\eta_t(r)$ are the turbulent diffusivities for the poloidal and

toroidal fields. The coefficient $\alpha(r,\theta)$ captures the generation of the poloidal field near the solar surface through the decay and dispersal of the tilted BMRs (Babcock–Leighton process) in our axisymmetric model.

In the regular model, the α has following form

$$\alpha(r,\theta) = \frac{\alpha_0}{4}\cos\theta\left[1+\mathrm{erf}\left(\frac{r-0.95R_\odot}{0.03R_\odot}\right)\right]\left[1-\mathrm{erf}\left(\frac{r-R_\odot}{0.03R_\odot}\right)\right] \tag{2.3}$$

where $\alpha_0 = 30$ m s^{-1}. In the Babcock–Leighton dynamo, the generation of the poloidal field involves some randomness, primarily due to scatter of BMR tilt around Joy's law and the random flux emergences. To capture these effects in our model, we include stochastic noise in the above α by replacing α_0 by $\alpha_0\,[1+\sigma(t,\tau_{\rm corr})]$, where $\sigma(t,\tau_{\rm corr})$ is a random number drawn from a uniform distribution in the range $[-1,1]$ and $\tau_{\rm corr}$ is the coherence time over which the value of α is constant. In all simulations, $\tau_{\rm corr} = 1$ month (typical lifetime of sunspots). With these parameters, the variations in the solar cycle remain consistent with what is seen in the last 300 years.

Here we discuss the profile of meridional circulation as it has been slightly modified here. The meridional circulation is obtained from a stream function ψ, such that $\rho\boldsymbol{v}_p = \nabla\times[\psi(r,\theta)\,\hat{\phi}]$, where $\rho = C\left(\frac{R}{r}-0.95\right)^{3/2}$, and

$$\psi r\sin\theta = \psi_0(r-R_p)\sin\left[\frac{\pi(r-R_p)}{(R_\odot-R_p)}\right]\{1-e^{-\beta_1\theta^\varepsilon}\}\{1-e^{-\beta_2(\theta-\pi/2)}\}e^{((r-r_0)/\Gamma)^2} \tag{2.4}$$

Here the values of the parameters are: $C = 0.407$ kg m^{-3}, $\beta_1 = 1.5\times10^{-8}$ m^{-1}, $\beta_2 = 1.3\times10^{-8}$ m^{-1}, $r_0 = (R_\odot - R_b)/3.5$, $\Gamma = 3.1\times10^8$ m, $R_p = 0.635R_\odot$, $R_b = 0.55R_\odot$.

We take two profiles for the meridional flows which we call MC1 and MC2. In MC1, we take $\varepsilon = 3$ and in MC2, we take $\varepsilon = 2$. These profiles are shown in Figure 2.2. This MC1 profile has been used in the work presented in Biswas et al. (2022). The profile MC2 has been used in many previous publications (Karak and Cameron, 2016; Karak and Choudhuri, 2011; Karak et al., 2018). This change makes the meridional circulation (MC1)

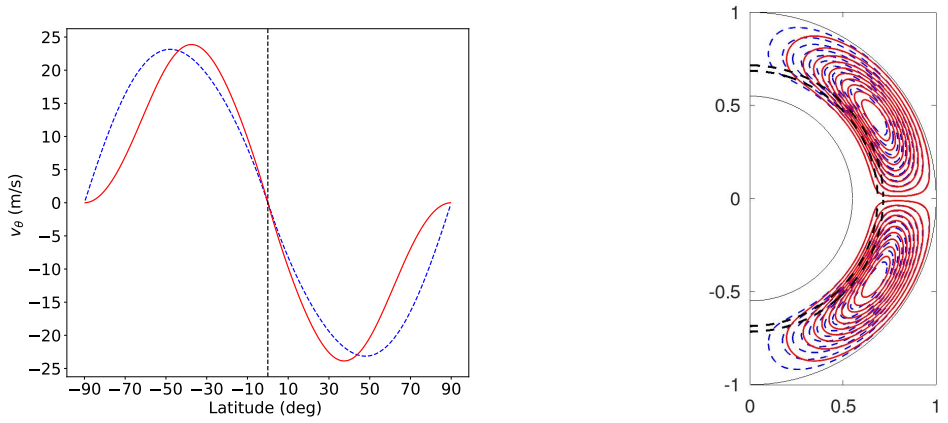

Fig. 2.2 The meridional circulation profiles used in the model. (Left) Shows the latitudinal variation of the surface meridional circulation and (right) shows its streamlines in the CZ. Red/solid and blue/dashed curves correspond to MC1 and MC2 profiles, respectively. Image Credit: Biswas et al. (2022)

to increase slightly at the lower latitudes and decrease at higher latitudes compared to the previous profile (MC2) (Chatterjee et al., 2004). With this slight modification in the flow, the equatorward migration of the sunspot belt is in better agreement with the observations. We will discuss the impact of this modification in further detail in the following section.

Finally, we describe the only nonlinearity that has been included in the model. The nonlinearity concerns the time at which flux is assumed to emerge. In every interval of 0.6 days, the code checks the amplitude of the toroidal field at each grid point above the base of the convection zone (BCZ). If the value is above a to-be-described critical value (B_c) then it is assumed that half of the flux emerges – its value at that grid point is halved and this half is added to the toroidal field near the surface at the same latitude keeping the toroidal flux conservation in mind. This is how the sunspot eruptions are modeled and this mechanism ensures that with each eruption a part of the toroidal flux from the CZ is lost. When the threshold is met, the toroidal flux is removed from the lower CZ so that it is no longer available to emerge at lower latitudes. This flux-loss associated with a threshold is the only nonlinearity we have included. As the process of flux loss is activated only

when the toroidal field strength meets a particular value (B_c), it is a significantly strong nonlinearity in the flux loss mechanism.

2.3 Results

We now discuss the results of the dynamo simulations. The latitudinal distribution of the surface radial field for eight cycles from a long run of 40 cycles is shown in Figure 2.3(a). We observe that this plot resembles the basic features of the solar cycle reasonably well (Charbonneau, 2020; Hathaway, 2015). We find that when $B_c = 0.8 \times 10^4$ G, the strength of the radial field on the surface is in agreement with the observed range Mordvinov et al. (2022a) and the subsurface flux loss through magnetic buoyancy becomes consistent with the observed flux loss through BMR emergences (Cameron and Schüssler, 2020). We use this value of B_c for the rest of the work.

We compute the model (pseudo) sunspot number by tracking the latitudes of eruptions of the toroidal flux (where the bottom field surpasses B_c) and with this number, we perform the same analyses as done in CS16 for the observed data. In Figure 2.3(c-d), we show that the latitudinal distribution of annual (model) sunspot emergence can be approximated with a Gaussian distribution.

The solar cycle variations of the total annual sunspot number and the width of sunspot distribution with the central latitudes of distribution are shown in Figure 2.4. Here we briefly describe the generic behaviour of the strong(red), moderate(blue) and weak(green) cycles. The strong cycles start from higher latitudes, rise rapidly, and reach their peak at a higher latitude whereas, the weaker cycles start lately from low latitudes, rise slowly and reach their peak when the toroidal belt has migrated towards much lower latitudes. Hence, the rise phase and maxima phase of these cycles are quite different depending on their strength. However, the statistical properties of all the cycles as shown in both the panels of

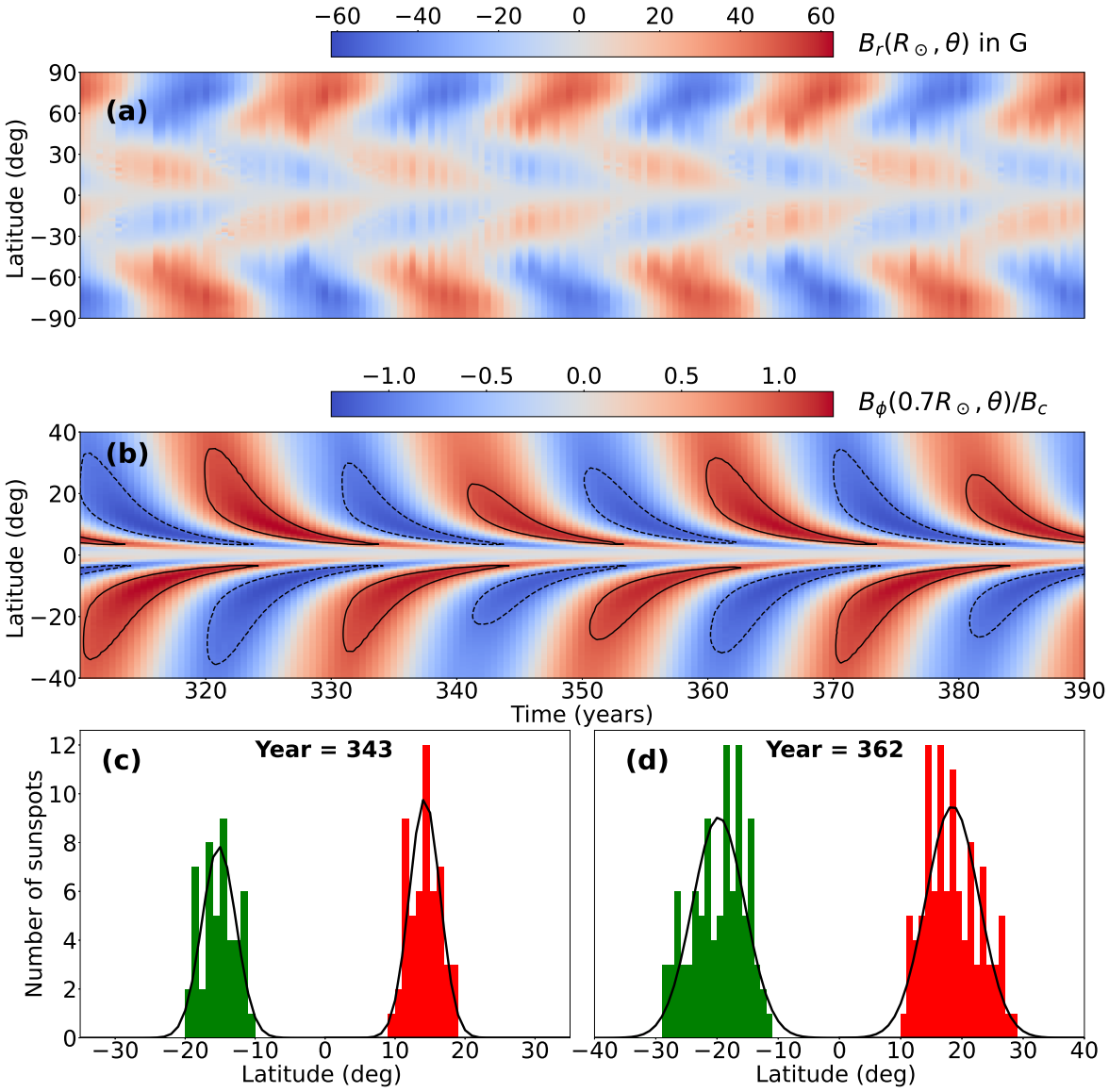

Fig. 2.3 A typical portion from our simulation. Latitudinal distributions of (a) the surface radial field and (b) the toroidal field at BCZ (the contour represents $B = B_c$, inside this contour the sunspots erupt in our model). (c) and (d) show the annual latitudinal distributions of sunspots for the years: 343 and 362, respectively and the fitted Gaussian profiles (black curves). Image Credit: Biswas et al. (2022)

Figure 2.4 tend to quickly converge just after their maxima and all the cycles decline in a similar manner. These behaviours largely agree with the observations (see Fig: of CS16).

We now explain these results based on the dynamo theory. In our model, cycles vary in strength due to the fluctuations introduced in the Babcock–Leighton α term. Suppose for some time α is large in a cycle, then a strong poloidal field will be produced in that cycle. The poloidal field is sheared by the differential rotation to produce the next cycle's toroidal field (we note that the shear is strongest at about 55° (Howe, 2009)). In our model, this toroidal field emerges once a critical threshold is reached, and gives rise to the (pseudo) sunspots on the solar surface. Further, the equatorward meridional circulation transports the toroidal field towards the equator making the sunspots emerge at lower and lower latitudes as the cycle evolves. Hence, as a high value of α in a cycle produces a strong poloidal field, this generates a strong toroidal field for the next cycle and the eruption condition ($B > B_c$) is satisfied at a wider latitudinal band early in the cycle when the field is at high latitudes. This explains why, for a strong cycle, sunspot starts appearing at high latitudes and the width of the latitude belt is large. On the other hand, when a cycle is weak, it takes a long time for the toroidal field to satisfy the spot-eruption condition by that time the meridional circulation drags the toroidal field towards the low latitudes. Hence, in a weak cycle, the sunspot belt begins at lower latitudes. The band of the sunspot latitudes is also narrow when the toroidal field is weak (as the spot eruption condition is satisfied only in a narrow latitude band).

Now we consider the effect of the loss of toroidal flux due to flux emergence (Cameron and Schüssler, 2020). Again we consider a strong cycle for which emergence begins early in the cycle at high latitudes. Each emergence reduces the subsurface toroidal flux (Cameron and Schüssler, 2020) so that a strong cycle which has many early flux emergences rapidly loses toroidal flux until the subsurface mean field strength is just above B_c. Thereafter the cycle begins to decline and the toroidal flux is advected equatorward

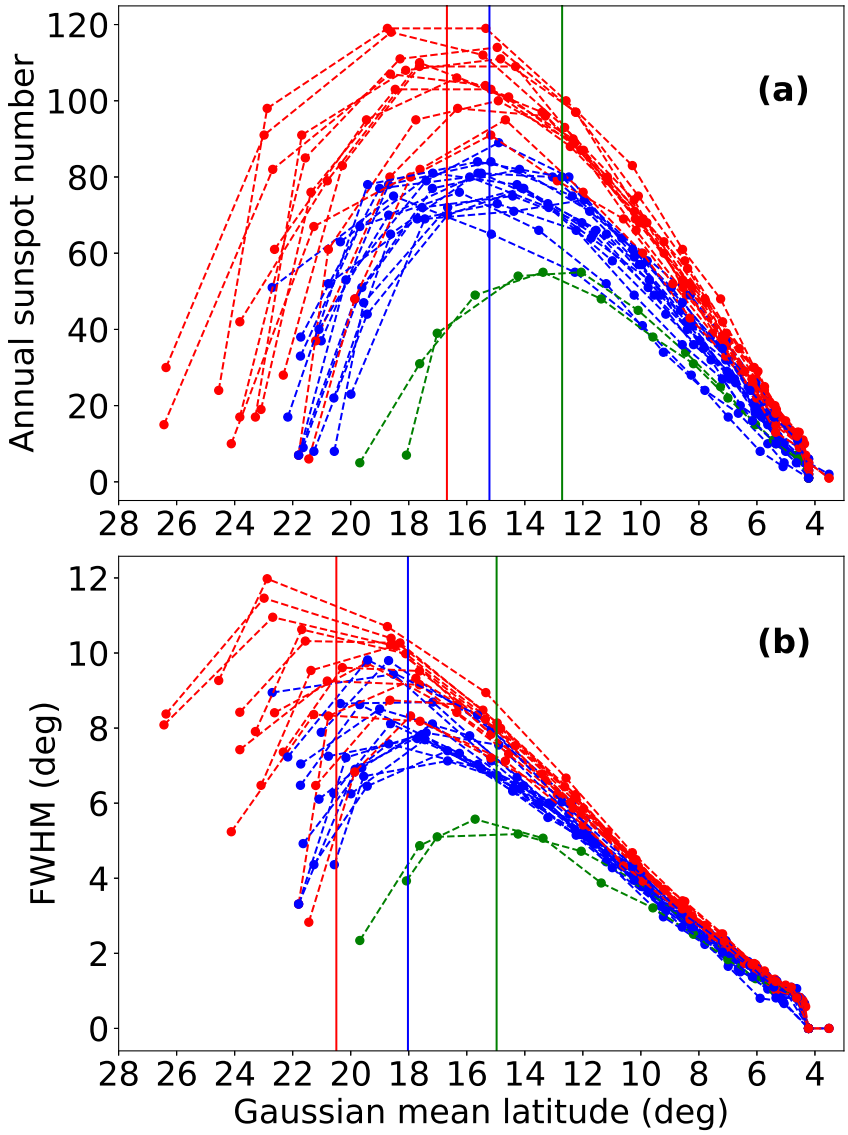

Fig. 2.4 (a) Model (pseudo) sunspot number for each year (based on the number of flux emergences) as a function of the central latitude of the Gaussian distribution. Different curves correspond to different cycles. (b) Same as (a) but for the distribution width (FWHM). Cycles begin at the left side of the plots and migrate to the right as they evolve. Vertical lines guide the average of the Gaussian-mean latitudes for strong (red), moderate (blue) and weak (green) cycles at their peaks. Image Credit: Biswas et al. (2022)

by the meridional flow while maintaining a strength just above B_c. The decrease in the meridional flow as we approach the equator will tend to increase the subsurface field strength, but this will be compensated for by further flux loss due to flux emergence.

On the other hand, in a weak cycle, there will be very few eruptions early in the cycle, and the field strength will simply build up as the flux is advected towards the stagnation point at the equator. At some point however the mean field will be comparable to B_c and the cycle will enter its decline phase. During this phase, the situation is entirely the same as for a strong cycle: the increase in the field strength as the flux builds up near the stagnation point is balanced by the loss of flux due to emergence, and the mean field strength is kept around B_c. A nonlinear process which causes flux emergence rates to be enhanced when the mean field exceeds B_c can explain why all cycles decline in the same way as evident from the right part of the curves in Figure 2.4. The value of $B_c = 0.8 \times 10^4$ G was chosen so that the model matches the observed range of the radial magnetic field on the solar surface and the amount of flux loss. Incidentally, this value is close to the equipartition field strength at BCZ ($\sim 10^4$ G). Although we did not choose the value of B_c keeping this in mind, it is interesting to note that just by constraining our model parameters through observations, we get a value of B_c, which is close to the equipartition field strength. A nonlinearity is expected because at this field strength the magnetic field has an energy density comparable to the kinetic energy density of the turbulent motions.

One quantitative discrepancy between our model presented in Figure 2.4(b) with respect to the observations (CS16) is that in the latter, we observe that as soon as the distance between the center of the Gaussian and the equator is roughly equal to the FWHM, all cycles begin to decay. The width of the butterfly wings is substantially smaller in our model; see Figure 2.4(b). In this work, we have been interested in investigating the role of flux loss in combination with a threshold for the emergence of active regions. For this pupose we have used a simple sharp threshold which involves two parameters B_c and

the fraction of flux which emerges when an emergence takes place. A better match with the observed widths might be possible if the flux emergence recipe had more degrees of freedom, however the basic physical idea is captured with this simple threshold. An additional possibility is that the butterfly wing widths are broadened by convective buffeting of the rising flux tubes before they reach the surface.

We have also studied the two aspects of Waldmeier effect, namely WE1 and WE2. WE1 refers to the anti-correlation between the rise time and the amplitude of the cycle, while WE2 refers to the positive correlation between the rise rate and the amplitude (Karak and Choudhuri, 2011). To check these features, we need to compute the rise rate, rise time and amplitude of the cycle. For this, we first smooth the three-month binned data using a Savitzky–Golay filter. Due to the overlap between the consecutive cycles, finding out the minimum is difficult. To avoid this problem we follow the same procedure as in Karak and Choudhuri (2011). We take the rise time as the time taken by a cycle to grow its activity from 20% to 80% of its peak value. The rise rate is computed by dividing the difference between values of 80% and 20% strength by the rise time. We find linear (Pearson) correlation coefficients -0.30 and 0.51 for these two cases (Figure 2.5). Thus the classical Waldmeier effect is also reproduced in this simulation. Earlier Karak and Choudhuri (2011) showed that fluctuations in meridional circulation are needed to reproduce WE1. Our result differs from this because WE1 is a weak anti-correlation and is sensitive to the way in which the data (and simulations) are treated. We find that a weak anti-correlation in WE1 exists even without including fluctuations in the meridional circulation. When fluctuation in meridional circulation is introduced, it enhances this anti-correlation. However, it leads to the model disagreeing with the fact that the widths of the sunspot latitude bands of all cycles are the same function of the central latitudes of the sunspot bands (CS16; Figure 2.4). Hence, observational features of sunspot cycle (Waldmeier, 1955) as analyzed in CS16

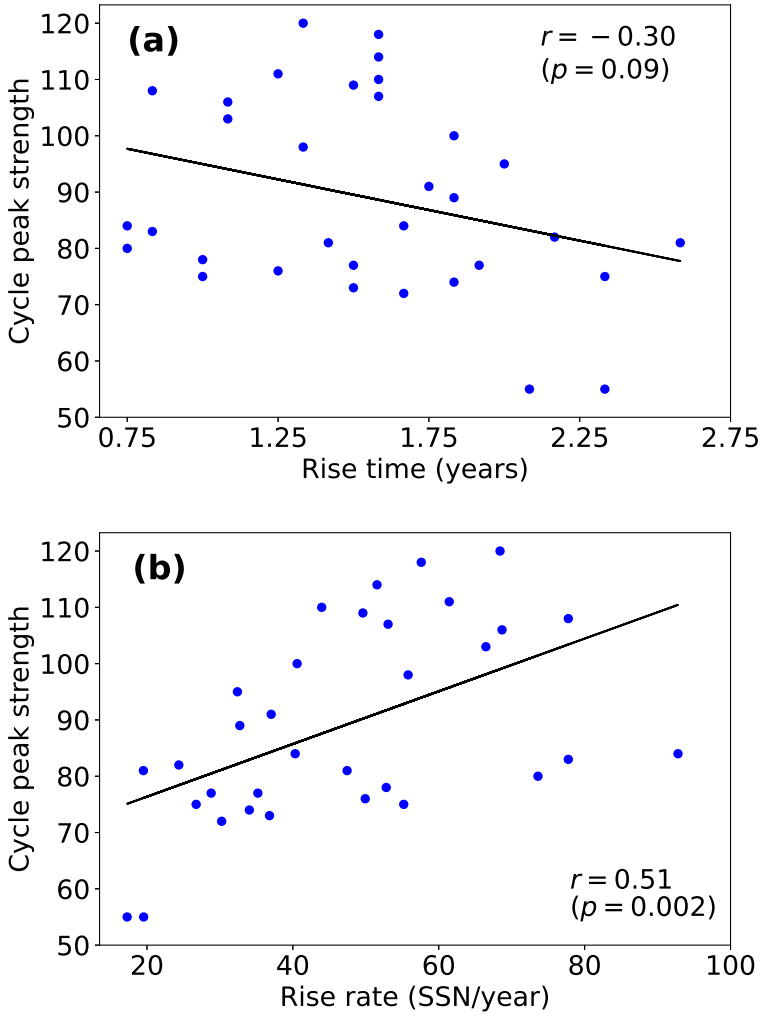

Fig. 2.5 The scatter plots between the peak of sunspot cycle (amplitude) and (a) the rise time and (b) the rise rate, i.e., WE1 and WE2, respectively. Image Credit: Biswas et al. (2022)

suggest that there was no large variation in the deep meridional circulation in the past 300 years.

From the previous explanation, we already got a hint that the equatorward drift of the meridional flow at low latitudes is important in shaping the trajectory of the sunspot band over the cycle. We find that if we make the equator-ward speed weaker in low latitudes, then the results become somewhat poor concerning its agreement with observations. In Figure 2.6, we show our results of the dynamo model in which the meridional circulation profile is changed to MC2 (see blue/dashed curves in Figure 2.2 for its profile). In this case, we notice that the agreement with observation is slightly poor, particularly, the butterfly wing begin at somewhat higher latitudes and the activity level of not all cycles strictly decline at the same rates.

So far in our model, we have ignored the delay induced due the rise of the magnetic flux from the BCZ to the surface. The magnetic buoyancy depends on the strength of the magnetic field at the BCZ and as a result the buoyancy induced delay in the source term of the poloidal field depends on magnetic field (Fan et al., 1994; Fournier et al., 2018). Here, we assume a simple inverse square relationship of the delay with the magnetic field strength such that the maximum delay is 6 months. The formula to incorporate this process in the code is following: $D = 180 \times (B_c/B)^2$, where D is the number of days taken by the flux tube to rise from the BCZ to the surface (i.e. the delay in flux eruption), B_c is the critical field strength to satisfy eruption condition and B is the value of toroidal field strength at the grid point where the eruption condition ($B > B_c$) has been met. In our simulations we however do not observe a significant change in the magnetic cycle due to the magnetic field dependent delay (results shown in Figure 2.7). The reason for this is that in this model, once the magnetic field B surpasses B_c the flux loss ($B \rightarrow B/2$) condition does not allow the magnetic field to increase too much higher than B_c and thus the buoyancy delay varies only a little. However, it is interesting to note that on an average the mediocre and

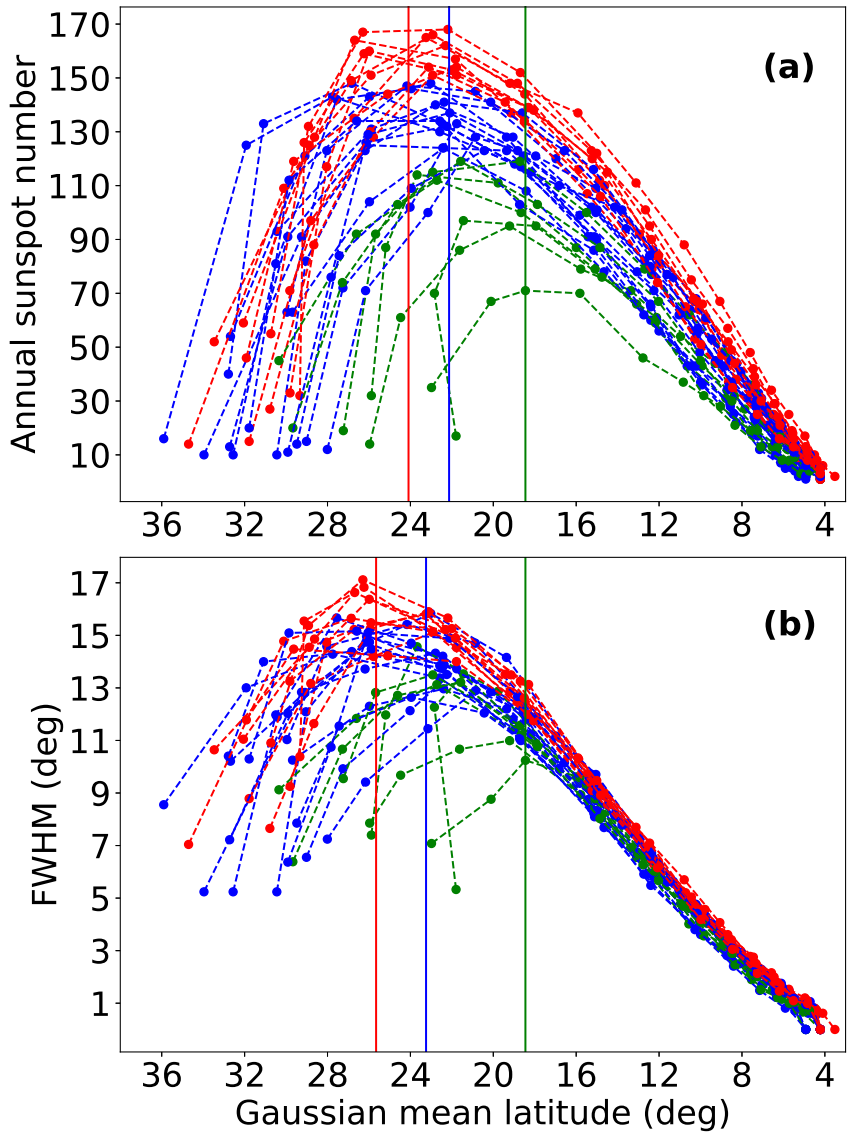

Fig. 2.6 Results obtained from a dynamo run with MC2 profile for the meridional flow (as shown by the blue/dashed line in Figure 2.2). Image Credit: Biswas et al. (2022)

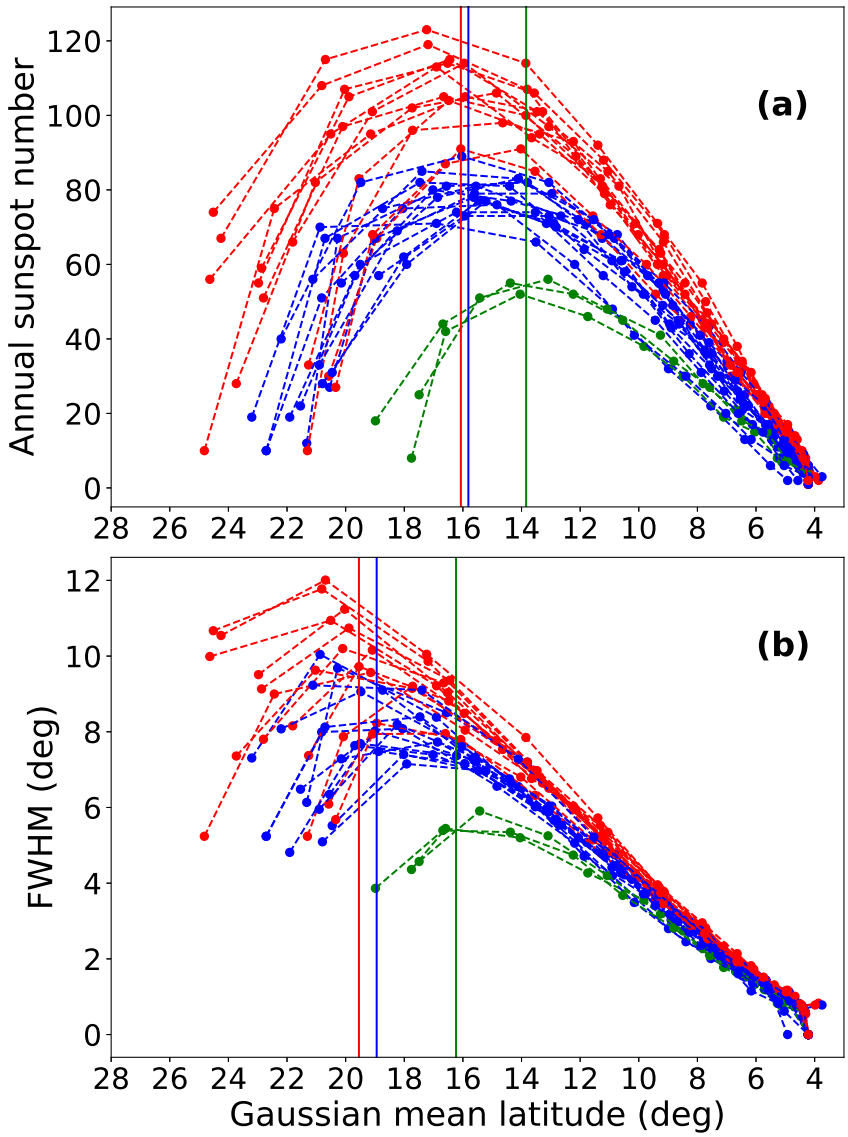

Fig. 2.7 Same as Figure 3 but here a delay has been included in the flux eruption process. Image Credit: Biswas et al. (2022)

the weaker cycles (blue and green ones, respectively) shift slightly towards high latitude regions. We note that the simulation presented here used the same initial condition that was used for the one presented in the Figure 2.4. The slight differences in the solutions (compare Figure 2.7 with Figure 2.4) are due to the time delay introduced in the flux emergence.

The nonlinearity to saturate the dynamo growth plays a critical role in reproducing the observed results. In our model, we have introduced nonlinearity only through magnetic buoyancy. Whenever the toroidal field tries to grow above a certain value, its value is reduced locally as it is moved to the surface. To investigate another nonlinearity, we have modified our model by no longer reducing the subsurface toroidal field to account for the flux lost due to emergence events and introduced a traditional α-quenching by replacing αB in Equation (2.1) with the following:

$$\frac{\alpha}{1+\left(\frac{\overline{B}}{B_c}\right)^2}\overline{B}(0.7R_\odot,\theta,t), \tag{2.5}$$

where $\overline{B}$ is the radially averaged toroidal magnetic field in the tachocline ranging from $0.68R_\odot$ to $0.71R_\odot$. This is basically a nonlocal treatment of poloidal source (Dikpati and Charbonneau, 1999).This treatment is known as the 'α-quenching' that mimics the nonlinearity named 'tilt quenching' (Jha et al. (2020), also see Chapter 3). The BMRs with higher magnetic fields rise quickly and the Coriolis force of the Sun gets less time to act on the flux tube, hence the tilts of those BMRs are lesser than the BMRs with weak magnetic fields. This dependence of BMR tilts with the magnetic field is known as the 'tilt quenching' and is captured in the dynamo simulations through the above-mentioned process of 'α quenching'.

The resulting magnetic field evolution and cycles from this case are very different from the case where the nonlinearity corresponds to flux emergence. The toroidal field

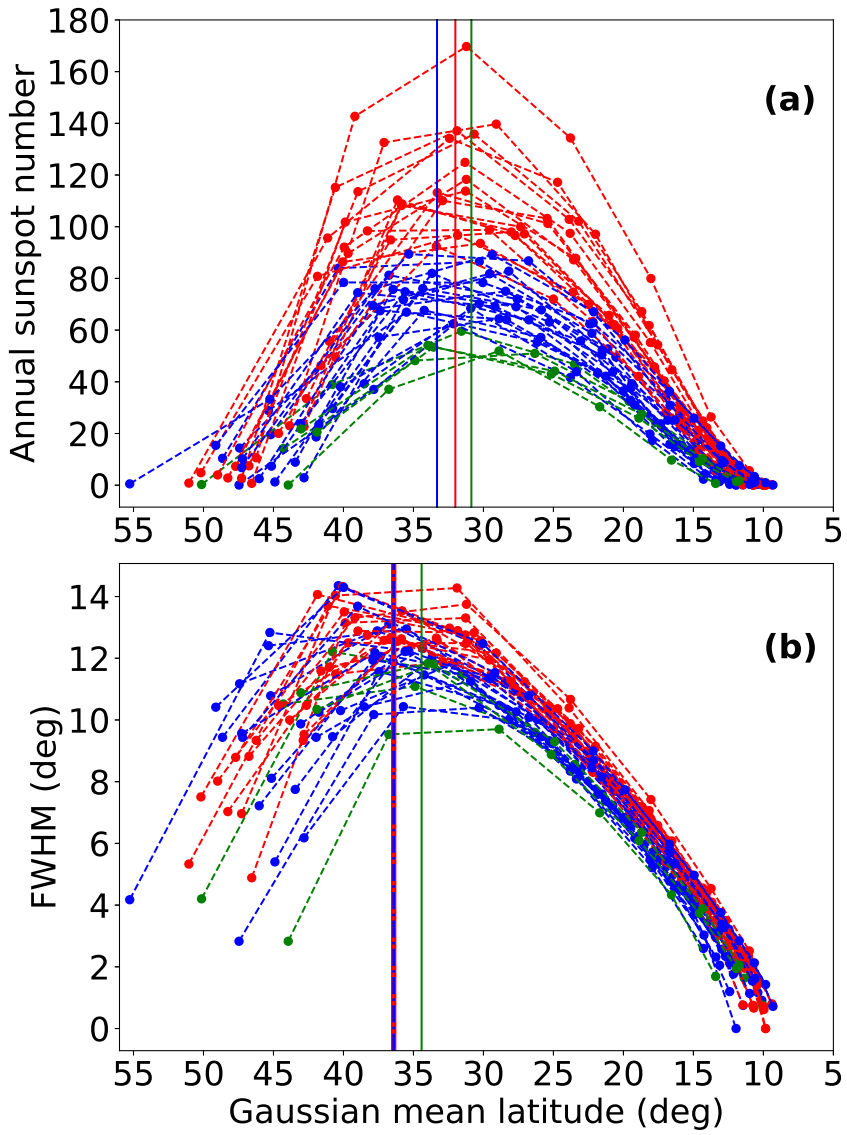

Fig. 2.8 Same as Figure 2.4 but obtained from a dynamo model in which the magnetic buoyancy is switched off and an α-quenching is introduced.

distribution is now spread all the way to very high latitudes and the cycle period becomes short; see Choudhuri et al. (2005) for a detailed analysis of this type of case. In this case, we find the condition $|B| > B_c$ being satisfied (giving model sunspots) all the way up to very high latitudes. To avoid the high latitude spots, we need to make the threshold for sunspot emergence latitude dependent (Karak, 2020) as follows

$$B_c(\theta) = B_c \exp|\,\theta - \frac{\pi}{2}\,|.$$

In Figure 2.8 we clearly see that in this model the activity level and the FWHM of all cycles start decreasing from the same central latitudes and they fall at different rates—this is in contradiction with the observations (CS16) and very different from the results of the dynamo model with magnetic buoyancy. We also note that Hazra et al. (2015) also failed to reproduce some features of the solar cycle when they stopped the toroidal flux loss in their dynamo model.

2.4 Conclusions

In conclusion, we have shown that the main features of the latitudinal distribution of sunspots as reported in Waldmeier (1955) and CS16 are reproduced in a Babcock–Leighton type flux transport dynamo model with stochastic fluctuations in the poloidal field source. We find that a constant equatorward flow near BCZ and a reduction of toroidal field due to flux emergence are essential to reproduce these results. Further, the critical strength of the mean magnetic field for the flux emergence through buoyancy is found to be of the order of 10^4 G. This is about the equipartition value where the magnetic energy density is equal to the kinetic energy density of the turbulent convective motions.